Effect of strain on electron mobility in graphene

Hideki Hirai, Matsuto Ogawa and Satofumi Souma[†]

Department of Electrical and Electronic Engineering, Kobe University, Kobe 657-8501, Japan

[†]email: ssouma@harbor.kobe-u.ac.jp

Abstract—We present a numerical study on the effect of mechanical strain on the electron mobility and the averaged electron velocity of graphene, where the graphene is assumed to be suspended and the phonon scattering is the dominant scattering mechanism. By employing the tight-binding formalism to describe the electronic band structure in the presence of strain and the Boltzmann transport equation to describe the non-equilibrium carrier transport in the presence of phonon scattering, the electron mobility was found to decrease nonlinearly with increasing the strain.

Fig. 1. (Left): Unit cell of graphene. (Right): Primitive lattice vectors $\boldsymbol{a}_1$, $\boldsymbol{a}_2$, and the three different hopping energies t_1, t_2, and t_3.

I. INTRODUCTION

Since the experimental success in the exfoliation of single layer graphene (SLG) in 2004, various graphene-based new functional devices have been proposed, including the bi-layer graphene transistors, graphene nanoribbon transistors, spin filters, gas sensors, pressure sensors, and so on [1]. Among them, the idea to engineer the electronic properties by introducing the mechanical deformation (strain) is especially important since it is one of special features which can be most flexibly designed if we use graphene as base materials [2], [3], [4], [5], [6], [7], [8]. One of the interesting device ideas based on the mechanically strained graphene is the "gapless switching" in locally strained graphene, where the strained induced shift of the Dirac point in the momentum space in one direction can cause the reflection (blocking) of electrons at the interface between the strained/unstrained graphene in spite of the absence of the bandgap in whole region. Such effect can also be interpreted as the effect of the pseudo magnetic field at the strained/unstrained interface region. It has been reported that such pseudo magnetic field mechanism can be utilized to realize the high on/off ratio in the strained graphene based FET, where even the steep subthreshold swing below 60 mV/decade is possible [4]. One important advantage of such locally strained graphene FET over other graphene-based FET such as graphene nanoribbon FET and the bilayer graphene FET is that in the channel region the Dirac-type linear (gapless) dispersion is maintained, suggesting that the high electron mobility – one of the most important benefit of using graphene – is maintained in the channel region. Nevertheless, the effect of strain on the electron mobility in graphene is not fully understood so far, although some pioneering studies have been reported [9], [10]. With such motivation, we study numerically the effect of mechanical strain on the electron mobility and the averaged electron velocity of graphene based on the semi-classical Boltzmann equation along with the tight-binding method, with taking into account the scattering due to the acoustic phonon and
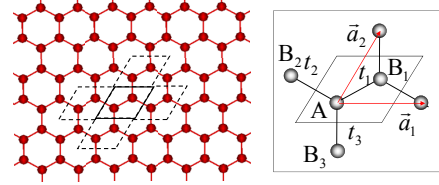
the optical phonon. Flexural (out-of-plane) phonon, which is important only in the absence of strain [10], [11], is not considered in the present study aiming at clarifying the role of conventional in-plane phonon modes.

II. THEORETICAL FORMALISM

A. Tight-binding formalism

Electronic properties of graphene can be determined using a unit cell containing two atoms (A and B), which are periodically arranged with the translational vectors $\boldsymbol{a}_1$ and $\boldsymbol{a}_2$. In the absence of strain, they are given by $\boldsymbol{a}_1 = {}^t(a_{1x}, a_{1y}) = {}^t(\sqrt{3}a_0, 0)$, and $\boldsymbol{a}_2 = {}^t(a_{2x}, a_{2y}) = {}^t(\sqrt{3}a_0/2, 3a_0/2)$ whereas the atomic positions of the A and B atoms in a unit cell are given, respectively, as $\boldsymbol{R}_{\mathrm{A}} = (0,0)$ and $\boldsymbol{R}_{\mathrm{B}} = (\sqrt{3}a_0/2, a_0/2)$. Here, a_0 is the spacing between nearest-neighbor atoms in unstrained graphene. In the presence of strain, these lattice vectors are modified to $\boldsymbol{a}'_n$ given by

$$a'_{ni} = \sum_{j=x,y} (\varepsilon_{ij} a_{nj} + \delta_{ij} a_{nj}), \qquad (1)$$

where δ_{ij} is Kronecker's delta, and ε_{ij} is the strain tensor. The position $\boldsymbol{R}_{\mathrm{B}} = (R_{\mathrm{B}x}, R_{\mathrm{B}y})$ of the B atom is also displaced by the strain according to the strain tensor ε_{ij}, so that $R_{\mathrm{B}i} = \sum_{j=x,y} (\varepsilon_{ij} R_{\mathrm{B}j} + \delta_{ij} R_{\mathrm{B}j})$.

Once the primitive lattice vectors and the atomic positions are given, the electronic band structures $\varepsilon_l(\boldsymbol{k})$ [$l = 1$ (2) corresponds to the valence (conduction) band] can be calculated by solving the eigenvalue problem

$$H(\boldsymbol{k}) |\psi_{l\boldsymbol{k}}\rangle = \varepsilon_l(\boldsymbol{k}) |\psi_{l\boldsymbol{k}}\rangle, \qquad (2)$$

with the $\boldsymbol{k}$-dependent Hamiltonian

$$\begin{aligned} H(\boldsymbol{k}) = H_0 &+ e^{-i\boldsymbol{k}\cdot\boldsymbol{a}_1} H_{-\boldsymbol{a}_1} + e^{-i\boldsymbol{k}\cdot\boldsymbol{a}_2} H_{-\boldsymbol{a}_2} \\ &+ e^{i\boldsymbol{k}\cdot\boldsymbol{a}_1} H_{\boldsymbol{a}_1} + e^{i\boldsymbol{k}\cdot\boldsymbol{a}_2} H_{\boldsymbol{a}_2}. \end{aligned} \qquad (3)$$

Here, H_0 is the intra cell Hamiltonian within a unit cell containing the A and B atoms, $H_{+(-)\boldsymbol{a}_1}$ is the hopping

Hamiltonian from a unit cell to the right (left) nearest-neighbor unit cell, and $H_{+(-)\boldsymbol{a}_2}$ is the hopping Hamiltonian from a unit cell to the upper (lower) nearest-eighbor unit cell (see Fig. 1). We employ the π-orbital model, in which only the p_z atomic orbital of each atom is taken into account to construct the atomistic Hamiltonian. Then, we can write

$$H_0 = \begin{pmatrix} \varepsilon_{2p} & -t_1 \\ -t_1 & \varepsilon_{2p} \end{pmatrix}, H_{\boldsymbol{a}_1} = H^\dagger_{-\boldsymbol{a}_1} = \begin{pmatrix} 0 & -t_2 \\ 0 & 0 \end{pmatrix},$$

$$H_{\boldsymbol{a}_2} = H^\dagger_{-\boldsymbol{a}_2} = \begin{pmatrix} 0 & -t_3 \\ 0 & 0 \end{pmatrix}. \tag{4}$$

where ε_{2p} is the on-site energy originating from the $2p_z$ atomic orbital, and is chosen to be zero. The three hopping energies t_1, t_2, and t_3 correspond to the three different inter atom distances shown in the right panel of Fig. 1. We note that $t_1 = t_2 = t_3$ in the unstrained or uniformly strained case. In our calculations, we employed the inter atom distance-dependent hopping energy $t_i = t(r_i) = t_0 e^{-\beta(r_i/a_0 - 1)}$, where $\beta = 3.37$, $r_i \equiv |\boldsymbol{R}_{B_i} - \boldsymbol{R}_A|$ is the distance between the A atom and its nearest-neighbor ith B atom (see Fig. 1), $a_0 = 0.1416$ nm is the inter atom distance in unstrained graphene [2], and $t_0 = 2.7$ eV is the magnitude of the hopping energy in unstrained graphene. When the strain is weak enough such that the hopping energy is modulated only within the linear order by strain, we can write

$$t_i = t_0 + \delta t_i,$$
$$\delta t_i = \left.\frac{dt(r)}{dr}\right|_{r=a_0} \delta a_i = t'(a_0)\delta a_i = -\beta t_0 \frac{\delta a_i}{a_0}, \tag{5}$$

where the change of the bond length δa_i is expressed using the strain tensor as

$$\delta a_1 = \varepsilon_{yy} a_0,$$
$$\delta a_{2(3)} = \left(\frac{3}{4}\varepsilon_{xx} + \sigma_{2(3)}\frac{\sqrt{3}}{2}\varepsilon_{xy} + \frac{1}{4}\varepsilon_{yy}\right) a_0, \tag{6}$$

with $\sigma_{2(3)} = + (-)$. In the case of uniformly strained case (i.e., $\varepsilon_{xx} = \varepsilon_{yy} = \varepsilon$, $\varepsilon_{xy} = \varepsilon_{yx} = 0$), the electronic states near the Fermi level $E_F = 0$ are described by the linear energy dispersion as $\varepsilon_l(\boldsymbol{k}) = (-1)^l \hbar v_F |\boldsymbol{k}|$, where v_F is the Fermi velocity and is expressed in the absence of the strain as $v_F^{(0)} \equiv 3a_0 t_0/2\hbar = 8.71 \times 10^7$ cm/s. In the presence of uniform strain, by using $a(\varepsilon) = a_0(1+\varepsilon)$ and $t(\varepsilon) = t_0(1-\beta\varepsilon)$ we obtained

$$v_F(\varepsilon) = v_F^{(0)}[1 + (1-\beta)\varepsilon - \beta\varepsilon^2], \tag{7}$$

which is approximately linear in ε for the strain $\varepsilon < 0.1$ considered in the present study. In the present study we focus only on the case of uniform strain.

B. Electronic transport formalism

1) Boltzmann equation and phonon scattering: In the present study, transport coefficients are calculated based on the Boltzmann equation, where the central quantity is the distribution function $f_l(\boldsymbol{k}, t)$, meaning the number of electrons occupied in the lth band for the wavevector $\boldsymbol{k}$ at a time t. Since we consider the spatially homogeneous system the distribution function does not have the position argument. In the presence of the electric field $\boldsymbol{E}$ and the scattering processes, the distribution function $f_l(\boldsymbol{k}, t)$ follows from the Boltzmann equation:

$$\frac{\partial f_l(\boldsymbol{k}, t)}{\partial t} + \frac{e\boldsymbol{E}}{\hbar} \cdot \frac{\partial f_l(\boldsymbol{k}, t)}{\partial \boldsymbol{k}} = R_l(\boldsymbol{k}, t). \tag{8}$$

Here the scattering term $R_l(\boldsymbol{k}, t)$ is calculated starting from the Fermi's golden rule as

$$R_l(\boldsymbol{k}, t) = \frac{1}{(2\pi)^2} \int_{BZ} dk'_x dk'_y$$
$$\times \left[W_l^{(ela)}(\boldsymbol{k}, \boldsymbol{k}'; t) + W_l^{(ine)}(\boldsymbol{k}, \boldsymbol{k}'; t) \right], \tag{9}$$

where $W_l^{(ela)}(\boldsymbol{k}, \boldsymbol{k}'; t)$ describes the elastic scattering contribution

$$W_l^{(ela)}(\boldsymbol{k}, \boldsymbol{k}'; t) = S_l^{(ela)}(\boldsymbol{k}, \boldsymbol{k}')\delta(\varepsilon_l(\boldsymbol{k}) - \varepsilon_l(\boldsymbol{k}'))$$
$$\times \left[f_l(\boldsymbol{k}', t) - f_l(\boldsymbol{k}, t) \right], \tag{10}$$

while $W_l^{(ine)}(\boldsymbol{k}, \boldsymbol{k}'; t)$ is the inelastic scattering contribution

$$W_l^{(ine)}(\boldsymbol{k}, \boldsymbol{k}'; t)$$
$$= \sum_{\sigma=\pm} \sum_{l'} \left[S_{\sigma,l\leftarrow l'}^{(ine)}(\boldsymbol{k}, \boldsymbol{k}')\delta(\varepsilon_l(\boldsymbol{k}) - \varepsilon_{l'}(\boldsymbol{k}') + \sigma\hbar\omega_{ph}) \right]$$
$$\times f_{l'}(\boldsymbol{k}', t)\left[1 - f_l(\boldsymbol{k}, t)\right]$$
$$- \sum_{\sigma=\pm} \sum_{l'} \left[S_{\sigma,l\rightarrow l'}^{(ine)}(\boldsymbol{k}, \boldsymbol{k}')\delta(\varepsilon_{l'}(\boldsymbol{k}') - \varepsilon_l(\boldsymbol{k}) + \sigma\hbar\omega_{ph}) \right]$$
$$\times f_l(\boldsymbol{k}, t)\left[1 - f_{l'}(\boldsymbol{k}', t)\right], \tag{11}$$

with the first and the second terms describing the "in-scattering" due to electrons entering into the state $(l, \boldsymbol{k})$ and the "out-scattering" due to electrons leaving from the state $(l, \boldsymbol{k})$, respectively. The sign $\sigma = +(-)$ means the phonon emission (absorption) process. We note that $S_{-,2\rightarrow1}^{(ine)} = S_{+,2\leftarrow1}^{(ine)} = S_{+,1\leftarrow2}^{(ine)} = S_{-,1\rightarrow2}^{(ine)} = 0$. In the above equation, the scattering functions S for elastic scattering, emission scattering, and the absorption scattering are given respectively as

$$S_l^{(ela)}(\boldsymbol{k}, \boldsymbol{k}') = C^{(ela)} |\langle\psi_{l\boldsymbol{k}}|\psi_{l\boldsymbol{k}'}\rangle|^2$$
$$S_{\sigma=+,l\leftarrow l'}^{(ine)}(\boldsymbol{k}, \boldsymbol{k}') = S_{\sigma=+,l\rightarrow l'}^{(ine)}(\boldsymbol{k}, \boldsymbol{k}')$$
$$= C^{(ine)} [N_B(\omega_{op}) + 1],$$
$$S_{\sigma=-,l\leftarrow l'}^{(ine)}(\boldsymbol{k}, \boldsymbol{k}') = S_{\sigma=-,l\rightarrow l'}^{(ine)}(\boldsymbol{k}, \boldsymbol{k}') = C^{(ine)} N_B(\omega_{op}), \tag{12}$$

where

$$C^{(ela)} = \frac{2\pi}{\hbar} \frac{E_D^2 k_B T}{2\rho_{mass} v_s^2}, \quad C^{(ine)} = \frac{2\pi}{\hbar} \frac{D_F^2 \hbar^2}{2\rho_{mass}\hbar\omega_{ph}}, \tag{13}$$

are the coefficients with the dimension [energy·length^2/time], with E_D being the deformation potential to characterize the acoutic phonon scattering, D_F the deformation field to characterize the optical phonon scattering. We employed $E_D = 4.5$ eV and $D_F = 1 \times 10^9$ eV/cm [12], [13]. $|\langle\psi_{l\boldsymbol{k}}|\psi_{l\boldsymbol{k}'}\rangle|^2$ accounts for the anisotropy factor originated from the pseudo spin symmetry [14], [15]. $N_B = 1/(e^{\hbar\omega_{op}/k_B T} - 1)$ is the

phonon occupation number. Other parameters are $\rho_{\mathrm{mass}} = 7.6 \times 10^{-8}$ g/cm^{-2} being the mass density in graphene, $v_{\mathrm{s}} = 2 \times 10^4$ m/s the sound velocity in the acoustic phonon dispersion, and $\hbar\omega_{\mathrm{ph}} = 164$ meV the optical phonon energy of the nearly constant optical phonon energy dispersion. Parameters E_{D}, D_{F}, ρ_{mass}, v_{s}, and $\hbar\omega_{\mathrm{ph}}$ are all strain dependent in general. However, in the present study we take into account the strain dependence only through v_{s} for acoustic phonon scattering and through $\hbar\omega_{\mathrm{ph}}$ for optical phonon scattering for simplicity. Sound velocity was calculated to decrease linearly with increasing the strain approximately as $v_{\mathrm{s}}(\varepsilon) = v_{\mathrm{s}}(1 - 2.5\varepsilon)$ [16], while the optical phonon energy was estimated to decrease approximately by 20 % by applying 10% strain [6], so that we roughly assumed $\omega_{\mathrm{op}}(\varepsilon) = \omega_{\mathrm{op}}(1 - 2\varepsilon)$, with ε being the ratio of uniformly applied strain.

2) Transport coefficient: In the present study, the Boltzmann equation was directly solved numerically employing the finite difference scheme assuming the initial distribution as being the equilibrium Fermi distribution. Once the distribution function is converged, the current density, carrier density, averaged velocity were calculated as

$$\langle \boldsymbol{J} \rangle = \frac{e}{(2\pi)^2} \sum_{l=1,2} \int_{\mathrm{BZ}} dk_x dk_y \boldsymbol{v}_l(\boldsymbol{k}) f_l(\boldsymbol{k}, t) = e \sum_{l=1,2} \langle n_l \rangle \langle \boldsymbol{v}_l \rangle, \tag{14}$$

$$\langle n_l \rangle = \frac{1}{(2\pi)^2} \int_{\mathrm{BZ}} dk_x dk_y \left[\delta_{l,1} + (-1)^l f_l(\boldsymbol{k}, t) \right], \tag{15}$$

$$\langle \boldsymbol{v}_l \rangle = \frac{1}{(2\pi)^2} \int_{\mathrm{BZ}} dk_x dk_y \boldsymbol{v}_l(\boldsymbol{k}) f_l(\boldsymbol{k}, t) / \langle n_l \rangle. \tag{16}$$

where $\boldsymbol{v}_l(\boldsymbol{k})$ is the group velocity of the lth band calculated as

$$\boldsymbol{v}_l(\boldsymbol{k}) = \frac{1}{\hbar} \frac{d\varepsilon_l(\boldsymbol{k})}{d\boldsymbol{k}} = \frac{1}{\hbar} \left\langle \psi_{l\boldsymbol{k}} \left| \frac{dH(\boldsymbol{k})}{d\boldsymbol{k}} \right| \psi_{l\boldsymbol{k}} \right\rangle. \tag{17}$$

In the enough low field condition where the converged average velocity can be regarded as linear in $\boldsymbol{E}$, the mobility μ was estimated by the relation $\langle \boldsymbol{v}_l \rangle = \mu_l \boldsymbol{E}$. where the proportionality constant μ_l is the mobility.

III. Results and discussions

Prior to the discussion on the effect of strain, we first show the results in the absence of strain. In Fig. 2 we show the electric field dependence of the converged average velocity for various electron densities: $n = 0.5 \times 10^{12}$ cm^{-2}, 1×10^{12} cm^{-2}, 2×10^{12} cm^{-2}, focusing on the lower field regime. The calculated average velocities increased rapidly first as the electric field is turned on, and saturated finally [12], [17], [18]. The negative differential conductance, observed in the lower electron density case, can be interpreted to be caused by the extremely weak scattering in the weak field regime (because of the small density of states) and the electric field induced increase of the optical phonon scattering events [18]. Next, the slope in the rapidly increasing regime, that is mobility, was steepest for lowest density case and became moderate with increasing electron density.
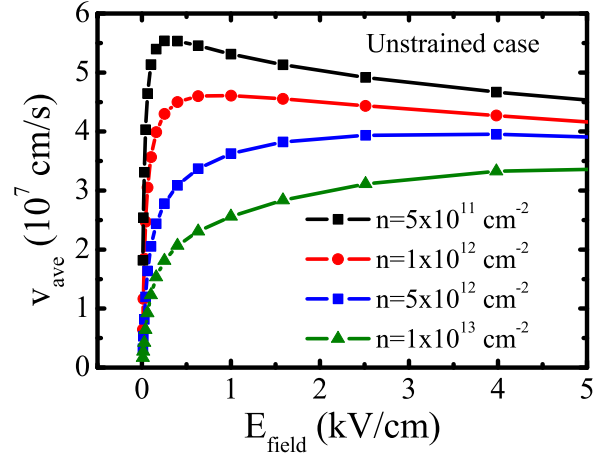
Fig. 2. Averaged velocity $\langle v_{l=2} \rangle$ for conduction band electron as function of the electric field. Results for various values of electron density are compared.
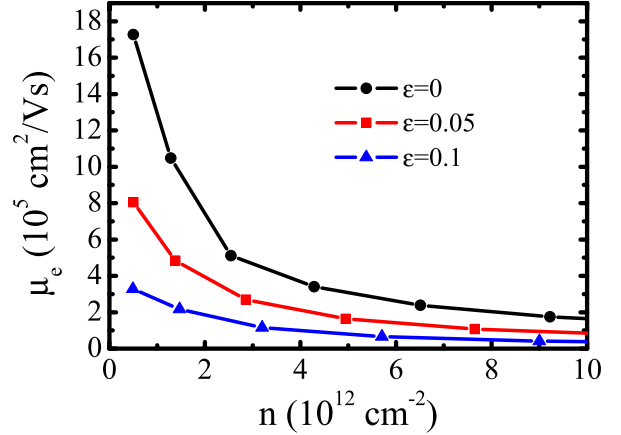
Fig. 3. Electron mobility as a function of the electron density. Results in the absence and the presence of the strain (uniform strain) are compared.

In Fig. 3 we plotted the electron mobility, evaluated from the slopes in the rapidly increasing regime in Fig. 1 (we evaluated them using the velocities at the electric field 0.01 kV/cm) together with the results in the presence of the strain. The value of mobility for low density $n = 0.5 \times 10^{12}$ cm^{-2} reached almost 2×10^6 cm^2/V·s. As increasing the electron density, the mobility decreased gradually, and became around 2×10^5 cm^2/V·s for $n \sim 10 \times 10^{12}$ cm^{-2}. The decrease of the mobility against the electron density was a result of increase in the scattering rate for electrons at the higher Fermi energy, which in turn is originated from the larger density of states and thus the larger numbers of final states. Figure 3 also exhibits that the mobility overall decrease the applying the strain.

Figure 4 shows the electron mobility as a function of the strain ratio ε for three different electron densities. Here it was seen that the mobility decreases nonlinearly with increasing the strain especially when the electron density is lower. One
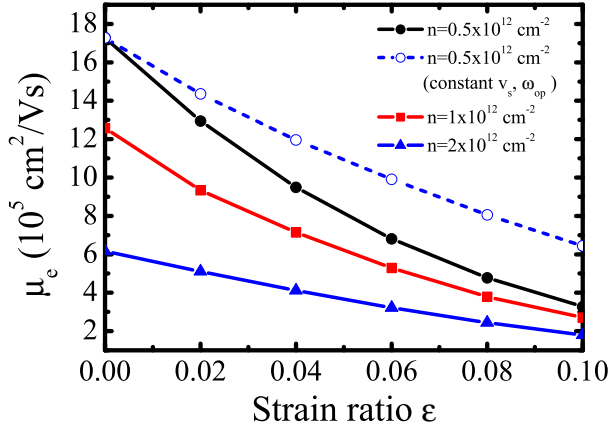
Fig. 4. Strain ratio dependence of the electron mobility for three different electron density. For comparison, results without taking into account the strain dependence of the sound velocity and the optical phonon energy are also plotted by dashed lines for $n = 5 \times 10^{11}$ cm^{-2}.
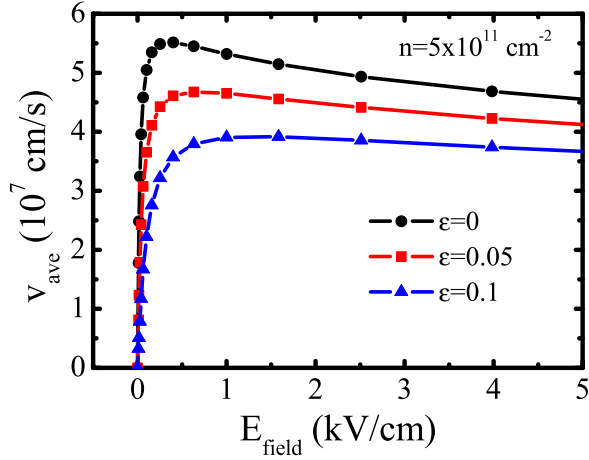
Fig. 5. Electric field dependence of the averaged electron velocity in the absence and the presence of the strain. Electron density was set to $n = 5 \times 10^{11}$ cm^{-2}.

of the possible origins behind the decrease of mobility is obviously the strain induced decrease of the Fermi velocity, which is expressed by Eq. (7) and is approximately linear for the small strain considered here, meaning that the decrease of the mobility seen in Fig. 4 was not only due to the decrease of the Fermi velocity. For comparison, the mobility without taking into account the strain dependence of the sound velocity and the optical phonon energy were also plotted in Fig. 4 by dashed line, which still indicated moderate nonlinear decrease and steeper than the decrease rate $[(1 - \beta)\varepsilon = -2.37\varepsilon]$ of Fermi velocity in Eq. (7), suggesting that the strain dependence of the phonon dispersion significantly influences the mobility. Moderate nonlinear behavior in constant v_s, ω_{op} model can be interpreted as being originated from the increase of scattering

rate, which in turn is caused by the increase of density of states via the increase of Fermi velocity.

Finally in Fig. 5 we compared the electric field dependence of the averaged electron velocity in the absence and the presence of the strain. Electron density was set to $n = 5 \times 10^{11}$ cm^{-2}. Here we found that the negative differential conductance seen in the low field regime for zero strain case was gradually diminished by increasing the strain. This is due to the strain induced enhancement of the scattering in the lower field regime discussed in Fig. 4. Also, the saturation velocity became smaller with increasing the strain. Such behavior can be interpreted as mainly caused by the decrease of the optical phonon energy due to strain.

IV. CONCLUSION

We studied numerically the effect of mechanical strain on the electron mobility and the averaged electron velocity of suspended (pristine) graphene, taking into account the electron-phonon scattering. By using the tight-binding formalism to calculate the electronic band structure in the presence of strain and the Boltzmann transport equation to calculate transport characteristics in the presence of phonon scattering, we found that the electron mobility decreases nonlinearly with increasing the strain, meaning that the strain influences the mobility not only through the decrease in the Fermi velocity but also through the increase in the phonon scattering events.

REFERENCES

[1] K. S. Novoselov, V. I. Fal'ko, L. Colombo, P. R. Gellert, M. G. Schwab, and K. Kim, Nature, **490**, 192 (2012).
[2] V. M. Pereira and A. H. Castro Neto, Phys. Rev. Lett. **103**, 046801 (2009).
[3] S. Souma, Y. Ohmi, and M. Ogawa, J. Comput. Electron. **12**, 170 (2013).
[4] S. Souma, M. Ueyama and M. Ogawa, Appl. Phys. Lett. **104** 213505 (2014).
[5] A. Mehdipour, K. Sasaoka, M. Ogawa and S. Souma, Jpn. J. Appl. Phys. **53** 115103 (2014).
[6] K. Tada, T. Funatani, S. Konabe, K. Sasaoka, M. Ogawa, S. Souma, and T. Yamamoto1, Jpn. J. Appl. Phys. **56**, 025102 (2017).
[7] Y.-H. Lee and Y.-J. Kim, Appl. Phys. Lett. **101**, 083102 (2012).
[8] H. Tomori, A. Kanda, H. Goto, Y. Ootuka, K. Tsukagoshi, S. Moriyama, E. Watanabe, and D. Tsuya, Appl. Phys. Exp. **4** 075102 (2011).
[9] R. Shah and T. M. G. Mohiuddin, Proceedings of the World Congress on Engineering 2011 Vol II (2011).
[10] E. Mariani and F. von Oppen, Phys. Rev. B**82**, 195403 (2010).
[11] T. Gunst, K. Kaasbjerg, and M. Brandbyge, Phys. Rev. Lett. **118**, 046601 (2017).
[12] H. Hirai, H. Tsuchiya, Y. Kamakura, N. Mori, and M. Ogawa, J. Appl. Phys. **116**, 083703 (2014).
[13] K. M. Borysenko, J. T. Mullen, E. A. Barry, S. Paul, Y. G. Semenov, J. M. Zavada, M. B. Nardelli, and K. W. Kim, Phys. Rev. B **81**, 121412(R) (2010).
[14] E. H. Hwang and S. Das Sarma, Phys. Rev. B**77**, 115449 (2008).
[15] T. Fang, A. Konar, H. Xing, and D. Jena, Phys. Rev. B**84**, 125450 (2011).
[16] Y. A. Baimova, S. V. Dmitriev, A. V. Savin, and Y. S. Kivshar', Physics of the Solid State **54**, 866 (2012).
[17] J. Chauhan and J. Guo, Appl. Phys. Lett. **95**, 023120 (2009).
[18] R. S. Shishir and D. K. Ferry, J. Phys.: Condens.. Matter **21** 344201 (2009).